Microporous and Mesoporous Materials 326 (2021) 111352

Contents lists available at ScienceDirect

Microporous and Mesoporous Materials

journal homepage: www.elsevier.com/locate/micromeso

Improving porosity and water uptake of aluminum metal-organic frameworks (Al-MOFs) as graphite oxide (GO) composites

Ülkü Kökçam-Demir, Niels Tannert, Marco Bengsch, Alex Spieß, Carsten Schlüsener, Sandra Nießing, Christoph Janiak *

Institut für Anorganische Chemie und Strukturchemie, Heinrich-Heine-Universität Düsseldorf, 40204, Düsseldorf, Germany

ARTICLE INFO

Keywords:
Metal-organic frameworks (MOFs)
Graphite oxide
Water sorption
Composite
Aluminum MOFs

ABSTRACT

Composites of the aluminum metal-organic frameworks (Al-MOFs) MIL-100(Al) and CAU-10-H and graphite oxide (GO) have been synthesized (by in-situ MOF formation) with four different GO loadings (from 2 to 16 wt%) for enhanced porosity and water uptake capacity. These composite materials MIL-100(Al)-GO and CAU-10-H-GO were examined by powder X-ray diffraction to show the retention of crystallinity and by scanning electron microscopy to show the retention of the morphology. Nitrogen and water sorption isotherms indicate no loss of mass-weighted surface areas, porosity and uptake capacity. In case of MIL-100(Al)-GO composites, the BET surface areas and porosities from nitrogen sorption data even reveal an increase of 8–12% in surface area with the GO increase from 2 to 9 wt% and an increase of 7–10% in total pore volume with GO loading from 9 to 2 wt %, in comparison to neat MIL-100(Al). In the 2 and 5 wt% CAU-10-H-GO composites, a 4% and 7% increase, respectively, in total pore volume was observed. The water uptake in the MIL-100(Al)-GO composites increased 23% over neat MIL-100(Al) with only 2 wt% GO but dropped again to a small 7% increase upon higher GO loadings up to 16 wt%. To the contrary, in the CAU-10-H-GO composites, the water uptake increases only slightly by 4–6% with 2–8 wt% GO. In particular, the MIL-100(Al)-GO composites showed an increase in the porosities and water uptake due to the synergistic effect from the interaction of MOF and GO with the formation of an additional interface with surface area and void volume. Furthermore, a hydrophilic shift of the water uptake to lower relative pressure $p \bullet p_0^{-1}$ was observed in the 2, 5, 8, 15 wt% CAU-10-H-GO composites. The MOF-GO composites showed essentially unchanged water sorption data after five water ad- and desorption cycles together with retention of crystallinity, morphology and porosity as verified by powder X-ray diffraction, scanning electron microscopy and by nitrogen sorption isotherm analysis, respectively.

1. Introduction

Metal-organic frameworks (MOFs) are infinitely extended coordination networks with metal nodes and bridging organic linkers [1–5]. They are promising candidates for applications such as gas sorption, including gas separation [6] and storage [6–8], catalysis [9–11], heat transformation [12–16].The adsorption performance of MOFs, such as its gas uptake capacity, can be still further improved by formulating them as composites with e.g. polymers [17,18], alumina [19–22], oxides [23], carbon nanotubes [24], functionalized graphite [25], or graphite oxide [26–31]. Graphite oxide (GO) is obtained by the oxidation of graphite [32]. It consists of graphene layers bearing various oxygen groups (carboxyl, hydroxyl, epoxy) on the basal planes and the edges of the layers [33,34]. Due to its hydrophilic character, GO disperses well in water or in some other polar solvents [35]. This carbon-based compound can be used for the preparation of hydrophilic composite materials.

MOF-GO composite materials (see Table S1, SI for a summary of applications) feature enhanced porosity and adsorption capacities of gases (compared to the pristine MOF and GO materials) for example in zinc [36,37], chromium [38,39] and copper [26,40,41]-based MOFs. For example, Elsayed et al. [38] achieved with MIL-101(Cr)-GO composites (2 wt% GO loading) a 10% higher BET surface area and a 22% increase in pore volume. In comparison, Yan et al. [31] reported for MIL-101(Cr)-GO composites (6 wt% GO loading) an approximately 26% higher BET surface area and a 35% increase in pore volume over neat MIL-101(Cr). Chen et al. [42] described an increase in the CO_2 uptake capacity and in the CO_2/CH_4 and CO_2/N_2 adsorption selectivities for MOF-505-GO composites with maximum values at 5 wt% GO loading.

* Corresponding author.
E-mail address: Christoph.Janiak@uni-duesseldorf.de (C. Janiak).

https://doi.org/10.1016/j.micromeso.2021.111352
Received 20 May 2021; Received in revised form 5 August 2021; Accepted 7 August 2021
Available online 12 August 2021

Wu et al. [43] synthesized MIL-68(Al)-GO composites for the removal of methyl orange (MO). They also showed that the MIL-68(Al) crystals grow between the planes of GO constructing a sandwich structure, which reflects a chemical interaction between MIL-68(Al) and GO. The composites exhibited better adsorption of MO than did both parent materials [43,44]. Notably, the adsorption performances of the MOF-GO composites are improved at low GO wt%, but higher GO loadings of over 10 wt% tend to have a detrimental effect [26,29,30,33,44,45].

For the MOF-GO composite formation an interaction between the oxygen groups of GO and the metal centers of MOFs at the outer MOF-particle surface is assumed [30]. In addition, hydrogen bonding from the donor hydroxyl groups on the GO to acceptor oxygen atoms in the MOF linker increases the degree of interaction between GO layers and MOF (Fig. S1, SI) [27,45]. In case of cubic MOF-5 and HKUST-1, perpendicular and parallel GO layers can coordinate to the MOF crystallites. Thereby the MOF crystallite can continue to grow in the non-GO-coordinated direction (Fig. S1, SI). In contrast, around the spherical MIL-100(Fe) crystallites, the GO layers coordinate with an angle larger or smaller than 90°. In the latter case, this coordination blocks the growth of the crystallites (Fig. S1, SI).

Water-based adsorption heat pumps (AHPs) and thermally driven adsorption chillers (TDCs) are recently advocated for the integration of MOFs in these applications [12,16,46–48]. AHPs and TDCs use adsorptive heat transformation and are based on the cycling adsorption and desorption of a working fluid at a highly porous substrate (Fig. S2, SI). Water is a desirable working fluid because of its non-harmful nature and large enthalpy change upon evaporation and condensation. MOFs used in AHPs/TDCs must be of extraordinary stability against the cycling sorption of the adsorbate, have an appropriate S-shaped sorption isotherm [47,49–51] and as high as possible adsorbate loading. Al-MOFs fulfill the requirements of stability and S-shaped isotherm [52,53] but their water uptake capacity of 300–400 mg g^{-1} is borderline for the desired application where the material should have an uptake of at least 300 mg g^{-1} [12,16,52,54]. Hence, measures or formulations to improve the water uptake capacity of Al-MOFs would be warranted.

In this work, we report on two Al-MOF-GO composites with the Al-MOFs MIL-100(Al) (MIL = Matériaux de l'Institute Lavoisier) and CAU-10-H (CAU = Christian-Albrechts-University) for improved H_2O adsorption relative to the individual components.

2. Experimental section

2.1. Materials and methods

All materials and solvents were commercially obtained and used without further purification. $AlCl_3{\cdot}6H_2O$ (99%) was purchased from Janssen Chemicals, $Al(NO_3)_3{\cdot}9H_2O$ (98–102%), basic aluminum acetate $Al(OH)(O_2CCH_3)_2{\cdot}H_2O$, graphite powder (99%) and isophthalic acid (H_2ipa, 99%) from Alfa Aesar, $Al_2(SO_4)_3{\cdot}18H_2O$ (>98%) from Sigma Aldrich, ethanol (p.a.) and H_2O_2 (30%) from Aldrich and Chemsolute, *N*, *N*′-dimethylformamide (DMF, p.a.) from Fischer Chemical, $KMnO_4$ (99%) from Grüssing GmbH, H_2SO_4 (95–97%) and $NaAlO_2$ (50–56%) from VWR Chemicals, $NaNO_3$ (99%) from PanReac AppliChem, SAPO-34 (silicoaluminiumphosphate) provided by Clarinat and trimesic acid (H_3btc, 98%) from abcr GmbH.

Elemental analyses (CHN) were performed using an Elementar Analysensysteme vario MICRO cube.

Fourier-transform infrared (FT-IR) measurement were carried out on a Bruker Tensor 37 IR spectrometer (Bruker Optics, Ettlingen, Germany) in the range of 4000 to 500 cm^{-1} with an ATR/KBr unit (Platinum ATR-QL, Diamond).

Scanning electron microscopy (SEM) images were acquired on a JEOL JSM-6510LV QSEM advanced electron microscope (Jeol, Akishima, Japan) using a LaB_6 cathode at 5–20 keV. The microscope was equipped with a Bruker XFlash 410 silicon drift detector (Bruker, Billerica, US) for energy-dispersive X-ray spectrometric (EDX) elemental analysis. Additional SEM images were acquired on a ZEISS LEO-1430 VP standard scanning electron microscope (Carl Zeiss AG, Jena, Germany) using a tungsten cathode.

Powder X-ray diffraction (PXRD) patterns were obtained at ambient temperature on a Bruker D2 phaser (Bruker, Billerica, US) using Cu-Kα radiation (λ = 1.54182 Å) between 5° < 2θ < 50° with a scan rate of 0.1502 down to 0.0142°/s, depending on the desired diffractogram quality (300 W, 30 kV, 10 mA). The diffractograms were obtained on a flat low-background silicon sample holder, for which the beam spot is strongly broadened at low angle so that only a fraction of the reflected radiation reaches the detector, hence the low relative intensities measured at 2θ < 7°. The analyses of the diffractograms were carried out with the "Match! 3.3.0" software.

Supercritical drying was carried out using a Leica EM CPD300 – automated critical point dryer which was set to perform 99 exchange cycles of CO_2.

Nitrogen (purity 99.9990%, 5.0) physisorption isotherms were measured on a Nova 4000e from Quantachrome at 77 K within the relative pressure range of $p{\bullet}p_0{}^{-1} = 10^{-3}$–1. Before the measurement the samples were degassed under vacuum (<10^{-2} mbar) at 120 °C for approx. 3 h (neat MIL-100(Al)), at 180 °C for approx. 3 h (neat CAU-10-H), at 60 °C for approx. 3 h plus a supercritical drying with CO_2 (99 cycles) (MOF-GO composite). All Brunauer-Emmett-Teller (BET [55]) surface areas were calculated from five adsorption points by applying Roquerol plots (r > 0.998). In this work we designate the surface areas from microporous MOFs which feature Type I isotherms as 'apparent S (BET)' based on the aforementioned reference [55], where it is noted that 'the BET-area derived from a Type I isotherm must not be treated as a realistic probe accessible surface area' but 'represents an apparent surface area, which may be regarded as a useful adsorbent "fingerprint" '. Total pore volumes were calculated from the nitrogen sorption isotherm at $p{\bullet}p_0{}^{-1} = 0.95$. Non-local density functional theory (NLDFT) calculations for the pore size distribution curves were done with the native 'NovaWin 11.03' software using the 'N_2 at 77 K on carbon, slit pore, NLDFT equilibrium' model [56–58].

Water sorption isotherms were obtained on a Quantachrome VStar4 device at 293 K within the partial pressure range of $p{\bullet}p_0{}^{-1} = 10^{-3}$–0.9. Before measuring of the isotherms, samples were degassed under vacuum (<10^{-3} mbar) at 120 °C for approx. 3 h (neat MIL-100(Al)), at 180 °C for approx. 3 h (neat CAU-10-H), at 60 °C for approx. 3 h (MOF-composite), using a FloVac degasser.

2.2. Synthesis of Al-based MOFs-GO composites

2.2.1. Preparation of GO

GO was synthesized by the Hummers and Offeman method as described in the literature [32], see SI. The resulting dark grey material is referred to as GO. For details see Figs. S3 and S4 and Tables S2, S3, SI.

2.2.2. Preparation of MIL-100(Al)

The microwave-assisted synthesis of MIL-100(Al) is based on the publication of Qiu et al. [59]. The parameters for the microwave synthesis were modified from this literature source. In a 10 mL microwave vessel, 132 mg (0.35 mmol) $Al(NO_3)_3{\cdot}9H_2O$, 61.2 mg (0.29 mmol) trimesic acid (H_3btc) and 3.1 mg (0.05 mmol) SAPO-34 were dissolved in 2 mL of distilled H_2O and stirred for 5 min. Then the reaction vessel was sealed, placed in a microwave reactor (CEM Discover, maximum power 300 W) and heated from room temperature (RT) to 190 °C within a few minutes (instrument operation: power of 150 W; autogenic pressure up to 20 bar). This temperature was maintained for 10 min. After cooling to RT, the as-synthesized product was centrifugated and washed with DMF (3 × 2 mL) and then the solvent was exchanged with ethanol (3 × 2 mL). The resulting material was dried in a vacuum oven at 120 °C for 3 h until a white powder was obtained. For details see Table S4, SI.

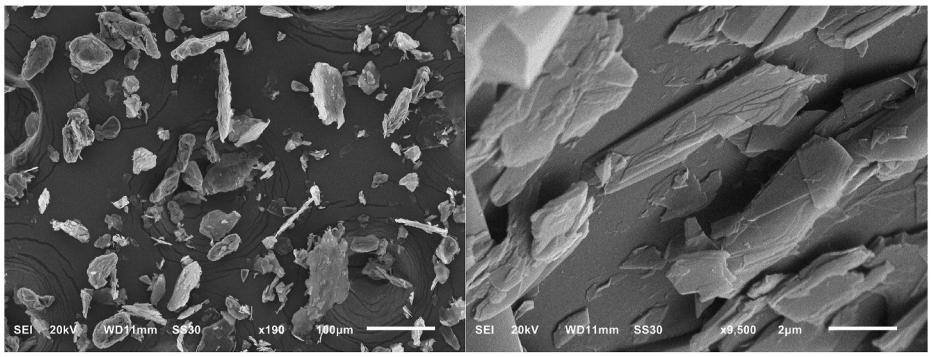

Fig. 1. SEM images of GO sheets at different magnifications.

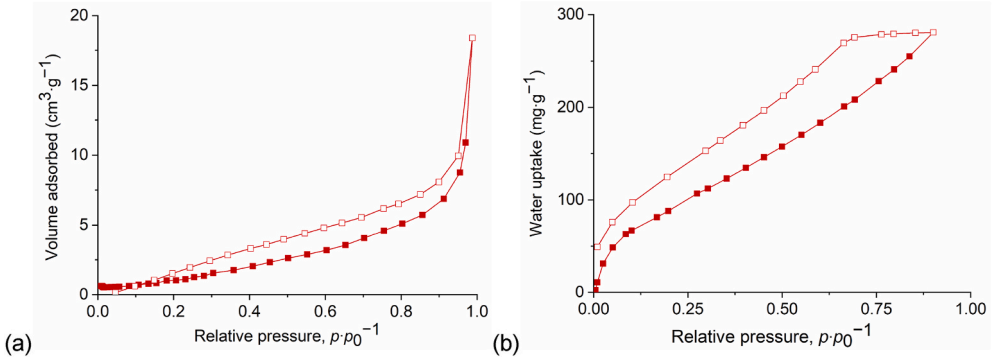

Fig. 2. N_2 (a) and H_2O (b) sorption isotherms of GO (at 77 K and 293 K, respectively).

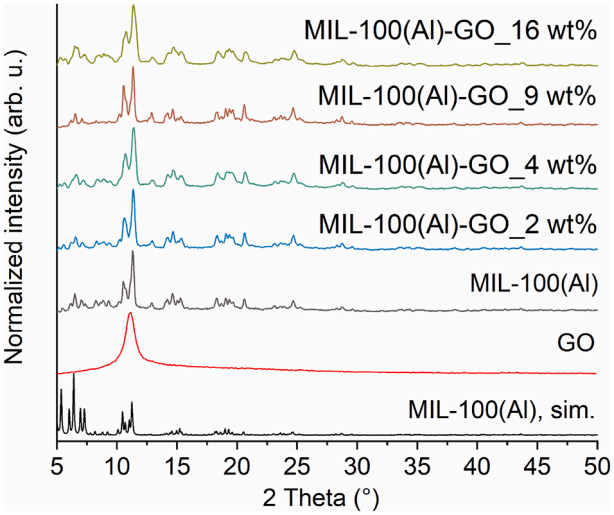

Fig. 3. Powder X-ray diffraction patterns of simulated MIL-100(Al) (CCDC no. 789872, CSD-Refcode BUSPIP) [66], GO, neat MIL-100(Al) and MIL-100 (Al)-GO_2, 4, 9, 16 wt% composites. The diffractograms were obtained on a flat "low background sample holder", for which the beam spot is strongly broadened at low angle so that only a fraction of the reflected radiation reaches the detector, hence the low relative intensities measured at $2\theta < 7°$.

2.2.3. Preparation of MIL-100(Al)-GO composites

The MIL-100(Al)-GO composites were synthesized under microwave irradiation method as described before. Hereby, GO (0.35, 1.05, 2, 3.6 mg) was added to the mixture of $Al(NO_3)_3{\cdot}9H_2O$ (132 mg, 0.35 mmol), H_3btc (61.2 mg, 0.29 mmol), SAPO-34 (3.1 mg, 0.05 mmol), and distilled H_2O (2 mL) and stirred at RT for 5 min (in 10 mL microwave vessel). Then the reaction vessel was sealed, placed in a microwave reactor (CEM Discover, maximum power 300 W) and heated from RT to 190 °C within a few minutes (instrument operation: power of 150 W; autogenic pressure up to 20 bar). This temperature was maintained for 10 min. After cooling to RT, the as-synthesized product was centrifugated and washed with DMF (3 × 2 mL) and then the solvent was exchanged with ethanol (3 × 2 mL). The resulting material was dried overnight in a vacuum oven at 60 °C until a light grey powder was obtained. GO (wt%) was calculated as follows: $(mass\ GO)\ /(mass\ MOF - GO) \times 100\%$. The added GO consisted of approx. 2, 4, 9, 16 wt% of the final materials. The resulting samples are referred to as MIL-100(Al)-GO_*x* (*x* = approx. 2, 4, 9, 16 wt%). For details see Scheme S1 and Table S4, SI.

2.2.4. Preparation of CAU-10-H

The synthesis of CAU-10-H is based on the publication of Reinsch et al. [60]. $AlCl_3{\cdot}6H_2O$ (482 mg, 2 mmol) and isophthalic acid (H_2ipa) (334 mg, 2 mmol) were reacted in a round bottom flask in distilled H_2O and DMF mixture (4:1, 10 mL) and refluxed at 135 °C for 24 h. After cooling to RT, the as-synthesized product was centrifugated and washed with DMF (40 mL) and then the solvent was exchanged with distilled water (2 × 40 mL). The resulting material was dried overnight in a vacuum oven at 60 °C until a white powder was obtained. For details see Table S5, SI.

2.2.5. Preparation of CAU-10-H-GO composites

The CAU-10-H-GO composites were synthesized under reflux. Hereby, GO (7, 20, 33, 66 mg) was added to the mixture of $AlCl_3{\cdot}6H_2O$ (483, 482, 484, 482 mg, 2 mmol), H_2ipa (335, 334, 335, 334 mg, 2 mmol) and distilled H_2O/DMF (10 mL; 4:1) solution. Then the round bottom flask was heated for 24 h at 135 °C under reflux. After cooling to RT, the as-synthesized product was centrifugated and washed with DMF (40 mL) and then the solvent was exchanged with distilled water (2 × 40 mL). The resulting material was dried overnight in a vacuum oven at 60 °C until a light grey powder was obtained. GO (wt%) was calculated

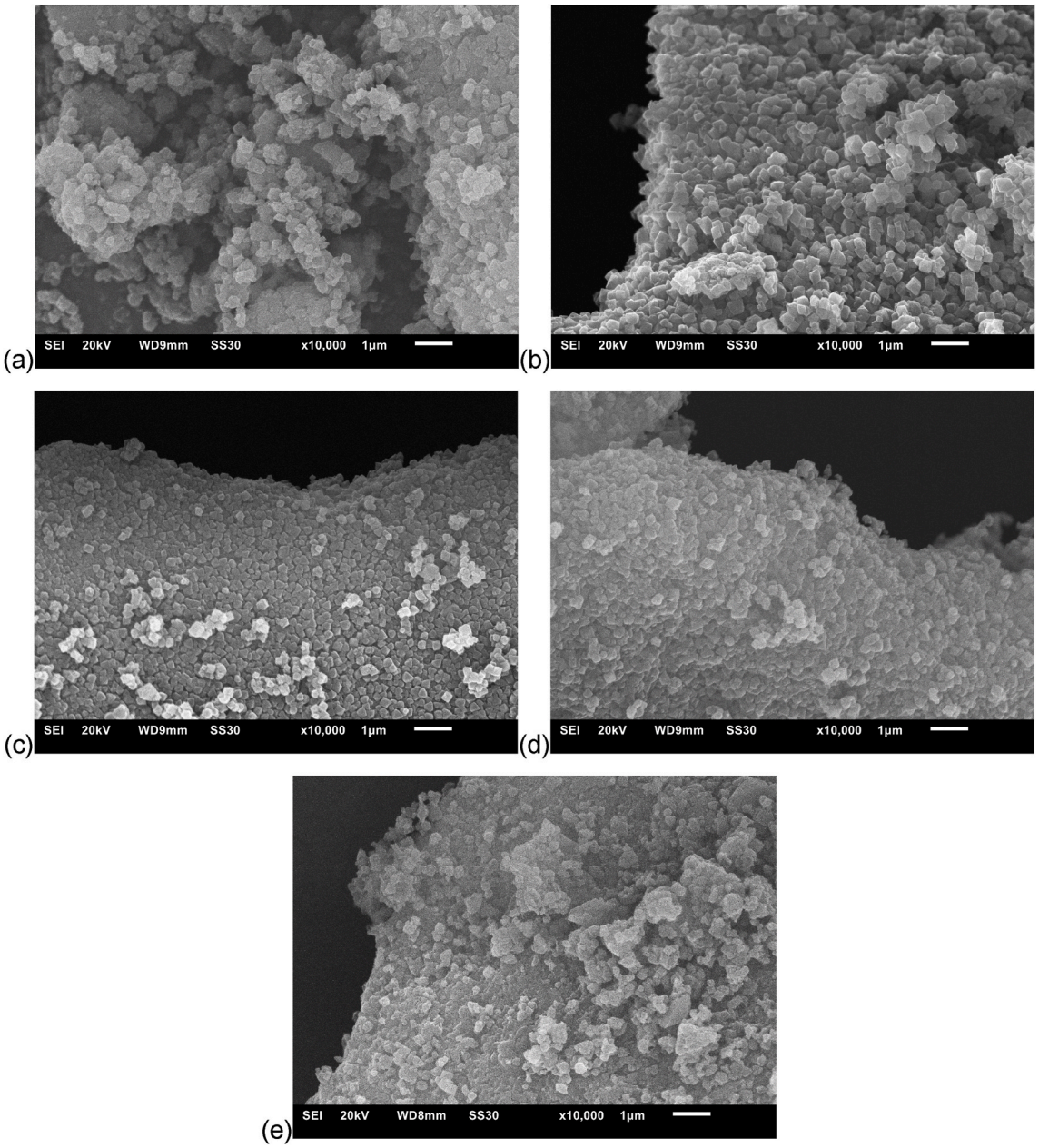

Fig. 4. SEM images of (a) neat MIL-100(Al), (b) MIL-100(Al)-GO_2 wt%, (c) MIL-100(Al)-GO_4 wt%, (d) MIL-100(Al)-GO_9 wt% and (e) MIL-100(Al)-GO_16 wt% (all scale bars 1 μm).

as follows: $(mass\ GO)\ /(mass\ MOF - GO) \times 100\%$. The added GO consisted of approx. 2, 5, 8, 15 wt% of the final materials. The resulting samples are referred to as CAU-10-H-GO_*x* (*x* = approx. 2, 5, 8, 15 wt%). For details see Scheme S2 and Table S5, SI.

3. Results and discussion

3.1. Graphite oxide, GO

Graphite oxide is a non-stoichiometric compound, which consists of planar carbon layers with sp^2 and sp^3 hybridized carbon atoms [26,61–63]. GO can be generated from graphite by the Hummers and Offeman method [32] through the addition of sodium nitrate, sulfuric acid and potassium permanganate. The oxidation of graphite introduces hydroxyl and epoxy functional groups at the formerly sp^2-hybridized graphite carbon atoms (Fig. S3, SI) [32]. Fig. 1 visualizes the morphology of the GO particles.

GO is thermally relatively unstable [64]. When GO is heated to above 150 °C the functional groups decompose into CO and CO_2 gas which exfoliates the layered GO structure into functionalized (thermally) reduced graphite oxide (TRGO, rGO) (see SI for details) [64,65]. Therefore, the final Al-MOF-GO composites were subsequently activated only at 60 °C for 3 h under vacuum.

GO has low micro- and mesoporosity. A Type III nitrogen adsorption isotherm with a Type H3 hysteresis (Fig. 2a) gives a BET surface area of 8 $m^2\ g^{-1}$. Type H3 loops are given by non-rigid aggregates of plate-like particles and also if the pore network consists of macropores [55]. The water adsorption isotherm (Fig. 2b) shows an uptake of 281 mg g^{-1} with an adsorption isotherm curvature indicative of a moderately hydrophilic meso-to macroporous material [16]. Noteworthy, the water adsorption isotherm at $p \cdot p_0^{-1} = 1$ still has a high positive slope and has not leveled off, which indicates an adsorption curve far from saturation, which will be reached only at higher pressures.

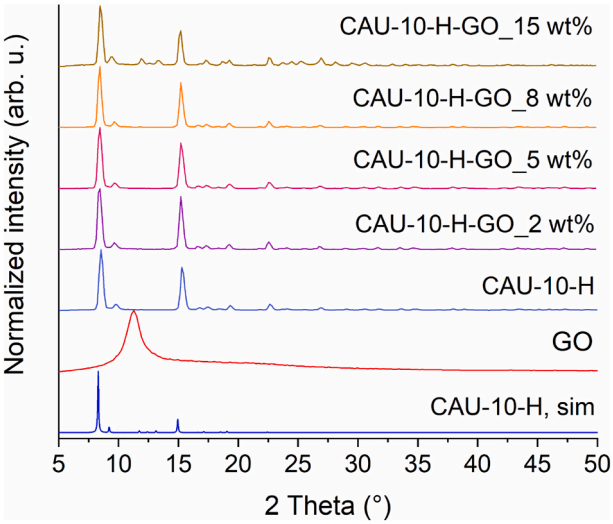

Fig. 5. Powder X-ray difraction patterns of simulated CAU-10-H (CCDC no. 1454066, CSD-Refcode OQOBUT) [67], GO, neat CAU-10-H and CAU-10-H-GO_2, 5, 8, 15 wt% composites. The diffractograms were obtained on a flat "low background sample holder", for which the beam spot is strongly broadened at low angle so that only a fraction of the reflected radiation reaches the detector, hence the lower relative intensities measured at $2\theta < 7°$.

3.2. MOF-GO composites

The MIL-100(Al)-GO composites were synthesized under microwave irradiation from GO, $Al(NO_3)_3{\cdot}9H_2O$, H_3btc, SAPO-34 and distilled water (see Exp. Section and Scheme S1, SI). From the photographic images in Fig. S6, SI, it can be seen that the colorless MIL-100(Al) and dark-grey GO combined to a grey to dark grey MIL-100(Al)-GO composites depending on the GO fraction. The PXRD patterns of the MIL-100 (Al)-GO composite materials (Fig. 3) verify the formation of MIL-100(Al) with identical crystallinity as neat MIL-100(Al). The characteristic broad peak of GO at 2-theta = 11° is not visible in the patterns of the MIL-100 (Al)-GO composites due to the low content of GO and the superposition of the relatively weak reflex from amorphous GO with the strong MIL-100(Al) reflections in this 2-theta region.

The SEM images of MIL-100(Al) and MIL-100(Al)-GO composites (Fig. 4, Fig. S7, SI) reveal similar tiny octahedrally-shaped crystals of 0.2–0.5 μm size [59] which for the MIL-100(Al)-GO composites, were grown on top of the GO particles, which can be viewed as a template for MOF crystallization (Fig. S7). Other work found that the hydroxyl, carboxyl, epoxy, ketone groups of GO can coordinate to the metal ions intended for the MOF and thus induce the growth of the MOF crystallites onto the GO layers [27]. It can be noted that the MIL-100(Al) crystallites form a dense layer on the GO which speaks for a powerful seeding action of the GO and a good adhesion of the formed MOF particles to the GO.

The CAU-10-H-GO composites were synthesized under reflux conditions from GO, $AlCl_3{\cdot}6H_2O$, H_2bdc and H_2O/DMF solution (see Exp. Section and Scheme S2, SI). The PXRD patterns of the CAU-10-H-GO composite materials (Fig. 5) indicate the formation of CAU-10-H with a crystallinity identical to neat CAU-10-H. The reflexes were retained unchanged and the characteristic broad peak of GO at 2-theta = 11° (Fig. 5) does not show in the composites, due to their low content of GO and the concomitant low intensity of the broad peak from amorphous GO (cf. Fig. 3).

The SEM images of the CAU-10-H-GO composites indicate that the CAU-10-H crystals were not exclusively grown on top of the GO particles (Fig. 6, Fig. S10, SI). In comparison with the SEM images of the MIL-100 (Al)-GO composites it is evident that the GO particles are not densely covered by the CAU-10-H crystallites. A significant amount of CAU-10-H also forms free from GO or does not adhere well and falls off afterwards (Fig. S10, SI). The particle size of the CAU-10-H composites is smaller than that of neat CAU-10-H.

3.2.1. Nitrogen sorption of MOF-GO composites

The isotherms of the composites and neat MIL-100(Al) are largely of Type Ib (Fig. 7) [55] according to the IUPAC (International Union of Pure and Applied Chemistry) classification, with the characteristic step for MIL-100(Al) before $p{\cdot}p_0^{-1} = 0.2$ indicating microporous windows and mesopores (Fig. S5, SI). The increase in gas sorption above $p{\cdot}p_0^{-1} = 0.9$ in a Type II or III branch is due to the filling of interparticle voids (Fig. 4). Among the MIL-100(Al)-GO composites the ones with 2, 4 and 9 wt% GO content had a higher BET surface area and a higher micropore volume than neat MIL-100(Al) which was prepared under the same conditions in this work (Table 1). The total pore volumes for the 2, 4 and 9 wt% MIL-100(Al)-GO composites were also slightly larger than for the MOF itself. Only the composite MIL-100(Al)-GO with 16 wt% GO content shows a lower porosity (Table 1) than neat MIL-100(Al). As GO has a negligible porosity, its content should decrease the porosity in a purely physical mixture. The counterintuitively observed increase in porosity from 2 to 9 wt% GO must be due to the interaction of the MIL and GO with the formation of an additional interface with surface area and void volume at this interface. Also, a composite of MIL-101(Cr)-GO had a higher BET surface area and pore volume compared to the neat MIL-101 sample which was ascribed to new pores formed between the graphene layers and MOF crystallites [69].

The isotherms of the CAU-10-H-GO composites and neat CAU-10-H at low relative pressure are of Type I [55] (Fig. 8), which is indicative of the microporous character. At $p{\cdot}p_0^{-1} > 0.9$ the isotherms show a Type II or Type III behavior [55], which indicates mesopores from interparticle voids. The BET surface areas of the composites CAU-10-H-GO with 2 and 5 wt% GO content appear slightly higher than for neat CAU-10-H but are still within experimental error. The CAU-10-H composites with 8 and 15 wt% GO content exhibit lower porosities than the MOF alone (Table 1). Different from the MIL-100(Al)-GO composites the formation of an interface surface area and pore volume is not evident in the CAU-10-H-GO composites.

3.2.2. H_2O-sorption

Fig. 9 depicts the S-shaped H_2O sorption isotherms of the MIL-100 (Al)-GO composites in comparison to neat MIL-100(Al). The characteristic two-step water-sorption isotherm of MIL-100(Al) with the steep and two-step rise is retained in the GO composites. The two-step curvature is due to the consecutive filling of to the two different mesopore sizes, first the 25 Å mesopores and then the 29 Å mesopores. The inflection point between the two pores is at $p{\cdot}p_0^{-1} \approx 0.36$ Fig. 9b) [50]. The composites with 2, 4, 9 and 16 wt% GO content have significantly higher water uptakes at $p{\cdot}p_0^{-1} = 0.5$, immediately after the loading lift, and at $p{\cdot}p_0^{-1} = 0.9$ than neat MIL-100(Al) (Fig. 9, Table 1). However, before $p{\cdot}p_0^{-1} \approx 0.31$ the water uptake of the composites is slightly less than that of neat MIL-100(Al) (Fig. 9b). The water adsorption performance of the MIL-100(Al)-GO composites is improved but most prominently with small GO loadings of 2 and 4 wt%, whereas for higher GO loadings of 9 and 16 wt% the improvement is less prominent and water uptake approaches the one of the neat MIL-100(Al) again. The PXRD patterns (Fig. S9, SI) and SEM images (Fig. S10, SI) indicate that the MIL-100 (Al)-GO composites were unchanged after water sorption.

Over the interesting uptake region starting from $p{\cdot}p_0^{-1} = 0.25$ GO takes up less water (due to its low porosity) than MIIL-100(Al) (Fig. 2, Fig. S8, SI). Hence, if one would estimate the water loading for a purely physical mixture as the sum of the mass-weighted vapor uptakes of MIL-100(Al) and GO such a physical mixture should have a lower water uptake than the neat MIL until $p{\cdot}p_0^{-1} = 0.9$. In the literature the adsorption of water vapor by MIL-101(Cr)-GO [31] and CO_2 by MOF-505-GO composites [42] was found to be enhanced over the neat MOFs. As was already seen for the porosity from N_2 sorption there is a synergistic effect from the interaction of the MOF with GO which

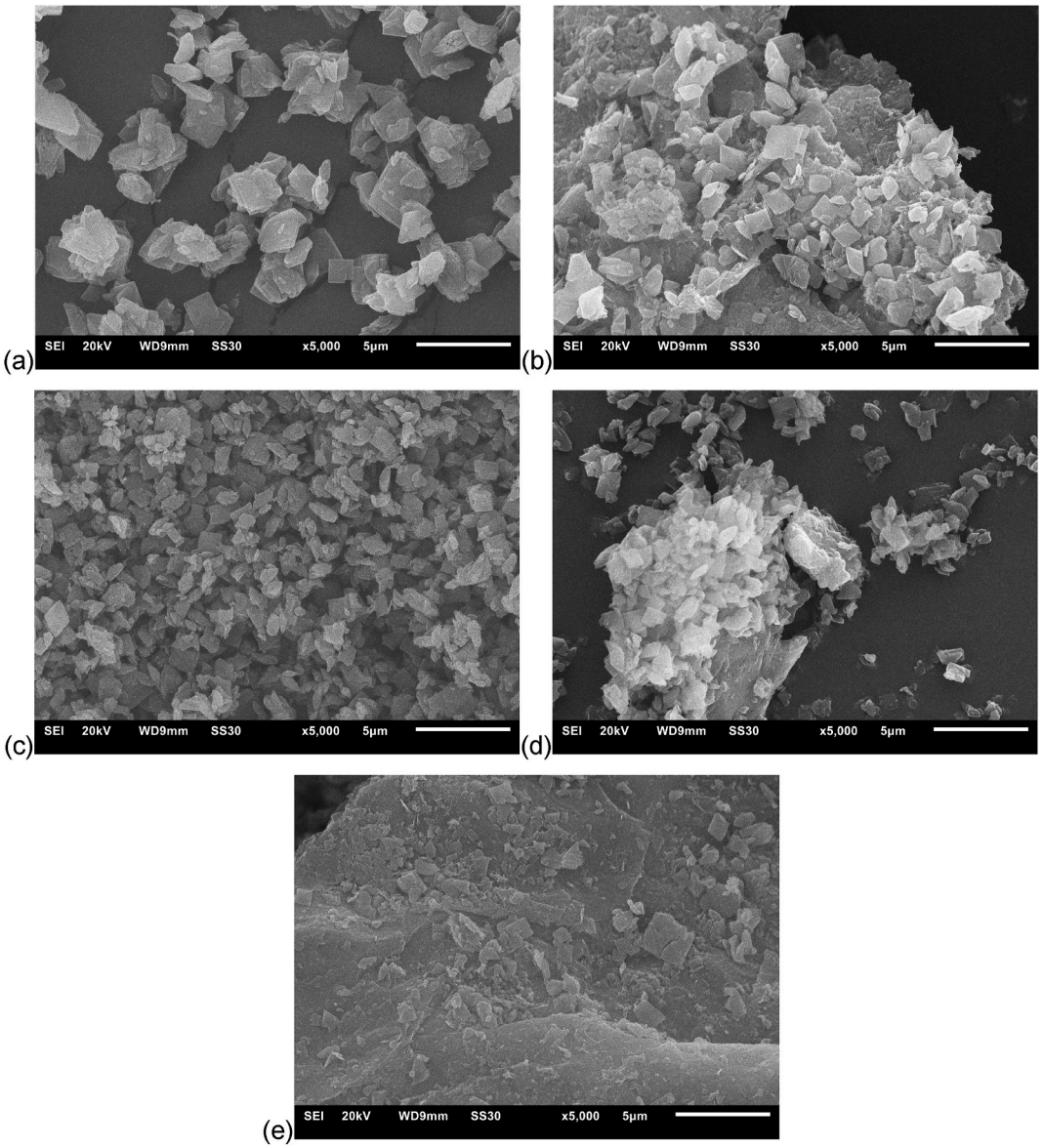

Fig. 6. SEM images of (a) neat CAU-10-H, (b) CAU-10-H-GO_2 wt%, (c) CAU-10-H-GO_5 wt%, (d) CAU-10-H-GO_8 wt% and (e) CAU-10-H-GO_15 wt% (all scale bars 5 μm).

amounts to additional pore volume available for water sorption above $p \cdot p_0^{-1} \approx 0.31$. Together the increase in porosity (by BET surface areas and pore volumes, see above) and water uptake of the MIL-100(Al)-GO composites can be reasoned by the apparently good interaction of MIL-100(Al) and GO without pore-blocking phenomena.

To analyze the effect of cycling water sorption on the MIL-100(Al)-GO composites, five water ad- and desorption cycles were performed using especially MIL-100(Al)-GO_2 and 4 wt% as examples. The water uptake values at $p \cdot p_0^{-1} = 0.5$ and 0.9 are the same within experimental error before and after the cycling (Fig. S13, Table S5). There is a slight increase in water uptake at $p \cdot p_0^{-1} = 0.3$ which may be attributed to hydrophilic sites becoming available, possibly due to very slight changes in the MOF structure, even if not reflected in the PXRD patterns (Fig. S11, SI), SEM (Fig. S12, SI) and N_2 sorption data (Table S5, SI) which remain rather identical. Only in case of MIL-100(Al)-GO_2 wt%, the BET surface area from nitrogen sorption data shows a positive increase of 12% after water sorption cycling. Hence, cycling water sorption may also have removed residual DMF or ethanol solvent from the synthesis.

Fig. 10 shows the S-shaped H_2O sorption isotherms of the CAU-10-H-GO composites in comparison to neat CAU-10-H. The curvature of the neat MOF is well retained in the composites. All isotherms exhibit a steep increase at $0.14 < p \cdot p_0^{-1} < 0.19$. The low hysteresis confirms the microporosity of the composites [55]. The composites with 2, 5, 8 wt% GO content have only very slightly higher water uptakes at $p \cdot p_0^{-1} = 0.9$, essentially still within experimental error to neat CAU-10-H (Table 1). Only the composite with 15 wt% GO content has again a significantly lower value (275 $m^2\ g^{-1}$) than neat CAU-10-H. Interestingly, the presence of GO shifts the steep increase in the S-shaped water adsorption isotherm from $p \cdot p_0^{-1} = \sim 0.17$ for neat CAU-10-H to $p \cdot p_0^{-1} = \sim 0.15$ with 2–15 wt% GO content. Consequently, the water uptake at $p \cdot p_0^{-1} = 0.15$ of these composites is significantly higher than that of neat CAU-10-H (Fig. 10b). Further, the steep water uptake of these composites is already mostly finished at $p \cdot p_0^{-1} = \sim 0.16$ before the uptake of neat CAU-10-H had even significantly started. The hydrophilic shift of the water uptake to lower relative pressure $p \cdot p_0^{-1}$ in the composites with 2–15 wt% GO content, compared to the neat MOF can be reasoned through the higher GO hydrophilicity in the low relative pressure region (Fig. S11, SI). Other than the small hydrophilic shift to slightly lower relative pressure there was no significant enhancement effect (also not

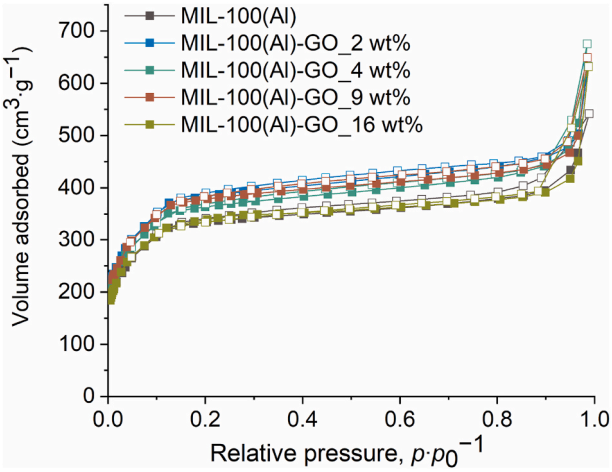

Fig. 7. N_2 sorption isotherms of neat MIL-100(Al) and MIL-100(Al)-GO_2, 4, 9, 16 wt% composites (at 77 K). Adsorption is depicted with filled, desorption with empty symbols.

for the porosity, see above) through the composite formation of the MOF CAU-10-H with GO. At present, possible amplification effects of MOF-GO composites cannot be predicted or necessarily expected. On the other hand, GO did not exert a negative effect, that is, no pore blocking on the MOF part.

Cycling water sorption on the CAU-10-H-GO composites was performed with the examples CAU-10-H-GO_2 and 5 wt%. Again, the water uptake values remain essentially identical after five water ad- and desorption cycling, except for a slight decrease at $p{\bullet}p_0{}^{-1} = 0.5$ for the 2 wt% composite (Fig. S21, Table S7, SI). After single and cycling water sorption (Fig. S17 and S19, SI), the PXRD patterns for the CAU-10-H-GO composites exhibit additional weak reflections which are due to residual water in the hydrophilic MOF, which was not dried before the PXRD measurements. The BET surface area from nitrogen sorption data remains within experimental error, which can be around ± 50 m^2 g^{-1} (Table S7, SI), however the curvature of the N_2 sorption isotherms after five water sorption cycles indicate additional mesoporosity, which is also reflected in an increased total pore volume. It is suggested that repeated water sorption enhances the interface or void volume between CAU-10-H and GO.

4. Conclusions

In this work, two novel MIL-100(Al)-GO and CAU-10-H-GO composites with graphite oxide (GO) contents from 2 to 16 wt% were prepared with in-situ MOF synthesis from the metal salts and linker in the presence of preformed GO under microwave irradiation (MIL-100(Al) and composites) and under reflux conditions (CAU-10-H and composites). Due to the good interaction of MIL-100(Al) and GO, the MIL-100 (Al)-GO composites largely showed an increase in adsorption capacity of nitrogen, in BET surface areas and (micro-)pore volumes and increased water uptakes. For the MOF CAU-10-H an effect of compounding with GO in terms of improved porosity and enhanced water uptake is minimal and hardly visible. Most prominently for the CAU-10-H-GO composites was a hydrophilic shift to slightly lower relative pressure $p{\bullet}p_0{}^{-1}$ of ~0.15 for the steep water uptake of the S-shaped isotherm compared to neat CAU-10-H with $p{\bullet}p_0{}^{-1}$ of ~0.17. Thus, an effect of GO on MOF porosity or sorption behavior cannot be generalized or predicted beforehand. MOF seeding and crystallite growth on the GO surface together with good MOF adhesion is suggested as crucial for a positive synergistic effect. Formation of an interface surface area, an interface volume and additional interparticle porosity is further suggested as the basis of a positive synergistic effect with enhanced porosity and guest uptake. Furthermore, the exemplifying MIL-100(Al)-GO_2 and 4 wt% as well as CAU-10-H-GO_2 and 5 wt% composites exhibit unchanged water uptakes without performance loss over more than five water ad- and desorption cycles.

Table 1
Results from N_2 and H_2O sorption measurements of MIL-100(Al)-GO and CAU-10-H-GO composites.

Sample[a]	S (BET) ($m^2{\bullet}g^{-1}$)[b]	$V_{pore(total)}$ ($cm^3{\bullet}g^{-1}$)[c]	$V_{pore(micro)}$ ($cm^3{\bullet}g^{-1}$)[d]	Water uptake ($mg{\bullet}g^{-1}$) at $p{\bullet}p_0{}^{-1}$ =		
				0.1/0.3	0.5	0.9
GO	8	0.01	–	67/112	158	281
				0.3	**0.5**	**0.9**
MIL-100(Al) Lit.	1576 [59]	n/a [59]	n/a [59]	≤200 [50]	≤400 [50]	500 [12, 50]
MIL-100(Al)	1317	0.67	0.44	273	429	492
MIL-100(Al)-GO_2	1416	0.74	0.49	234	543	606
MIL-100(Al)-GO_4	1423	0.73	0.46	268	503	570
MIL-100(Al)-GO_9	1477	0.72	0.49	211	465	531
MIL-100(Al)-GO_16	1287	0.65	0.46	213	458	526
				0.15	**0.3**	**0.9**
CAU-10-H Lit.	635 [60]	n/a [60]	0.25[e] [60]	≤5 [68]	≤270 [68]	340 [67, 68]
CAU-10-H	666	0.28	0.24	8	275	331
CAU-10-H-GO_2	671	0.29	0.23	181	278	345
CAU-10-H-GO_5	689	0.30	0.24	83	260	350
CAU-10-H-GO_8	589	0.28	0.20	146	255	345
CAU-10-H-GO_15	564	0.26	0.19	127	219	272

All values are rounded.

[a] In MIL-100(Al)-GO_*x* or CAU-10-H-GO_*x* "*x*" refers to the wt% of GO in the composite (see Exp. Section). For example, MIL-100(Al)-GO_2 has 2 wt% loading of GO in the composite.

[b] Apparent *S*(BET) values were determined from N_2 sorption isotherms at 77 K. *S*(BET) were obtained from five adsorption points in the pressure range of $0.04 < p{\bullet}p_0{}^{-1} < 0.1$ for MIL-100(Al), $0.01 < p{\bullet}p_0{}^{-1} < 0.4$ for MIL-100(Al)-GO_*x* composites, $0.01 < p{\bullet}p_0{}^{-1} < 0.02$ for CAU-10-H and $0.01 < p{\bullet}p_0{}^{-1} < 0.4$ for CAU-10-H-GO_*x* composites.

[c] Total pore volume, $V_{pore(total)}$ calculated from N_2 sorption isotherm at 77 K ($p{\bullet}p_0{}^{-1} = 0.95$ for MIL-100(Al) corresponding composites, and $p{\bullet}p_0{}^{-1} = 0.90$ for CAU-10-H and corresponding composites) for pores ≤ 20 nm.

[d] Micropore volume, $V_{pore(micro)}$ refers to the volume that originates only from micropores, obtained by the *V*–*t* method with thickness method "DeBoer" in the range of $0.2 < p{\bullet}p_0{}^{-1} < 0.4$ for MIL-100(Al), MIL-100(Al)-GO_*x* composites, CAU-10-H and CAU-10-H-GO_*x*. All correlation coefficients (*r*) within calculations were ≥0.999.

[e] Micropore volume determined by single point calculation at $p{\bullet}p_0{}^{-1} = 0.5$.

Credit authorship contribution statement

Ülkü Kökçam-Demir: performed the experiments, collected and interpreted the data, wrote and revised the manuscript, outlined the idea together. **Niels Tannert:** carried out preliminary experiments, outlined

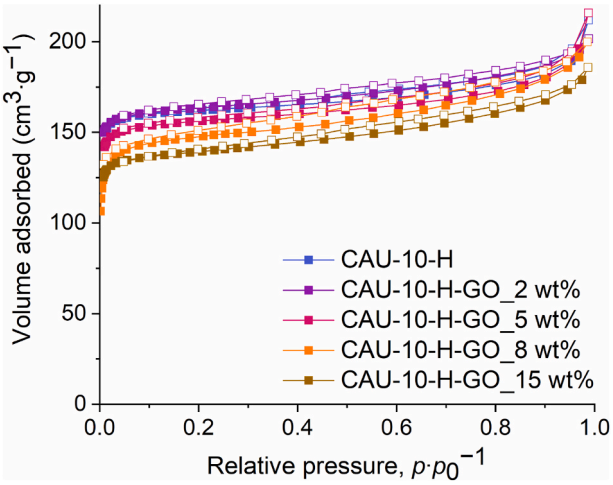

Fig. 8. N_2 sorption isotherms of neat CAU-10-H and CAU-10-H-GO_2, 5, 8, 15 wt% composites (at 77 K). Adsorption is depicted with filled, desorption with empty symbols.

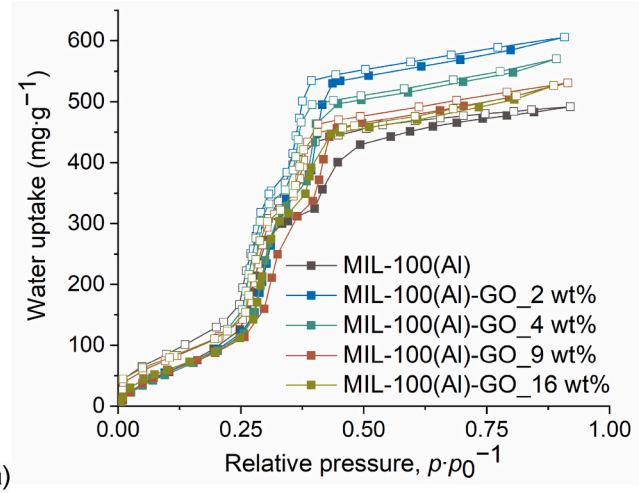

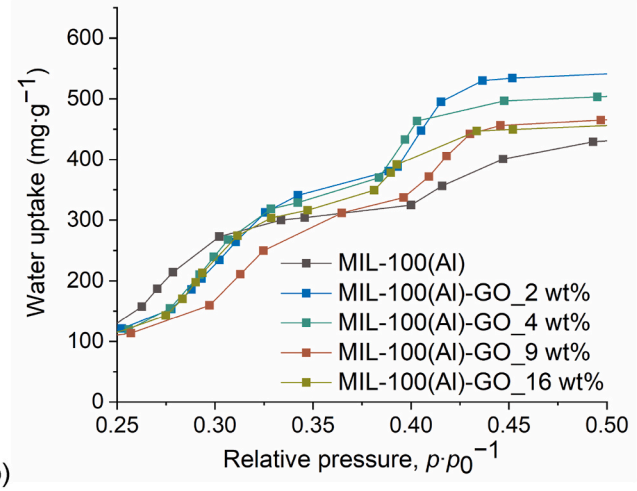

Fig. 9. Water sorption isotherms of neat MIL-100(Al) and MIL-100(Al)-GO_2, 4, 9, 16 wt% composites (at 293 K). Adsorption is depicted with filled, desorption with empty symbols. (a) Full region from p•p_0^{-1} = 0–1, (b) expanded adsorption region from p•p_0^{-1} = 0.25–0.5 (for clarity, only the adsorption isotherms are shown).

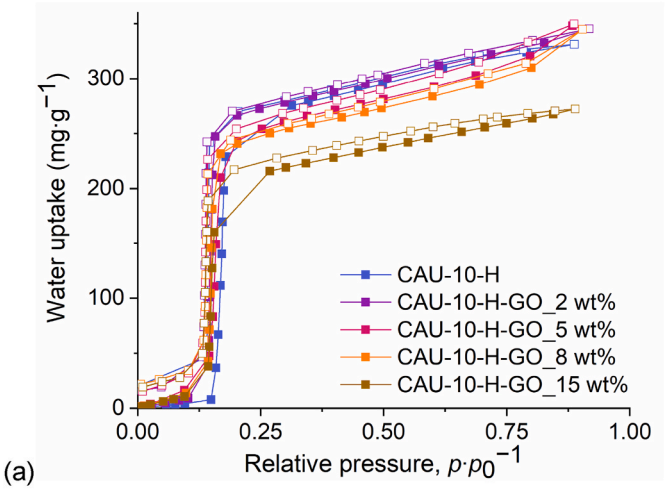

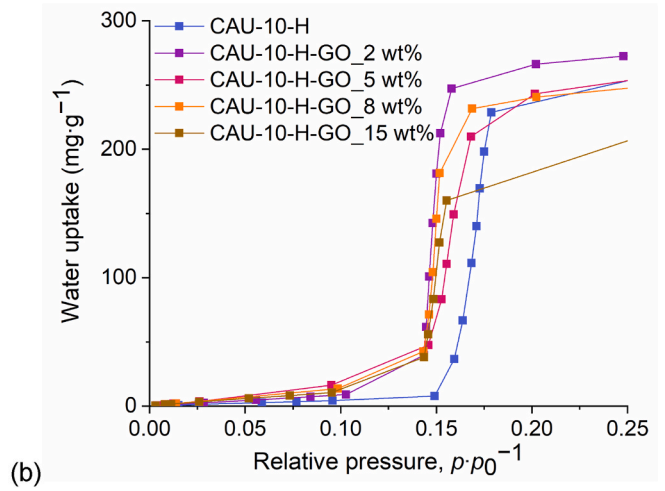

Fig. 10. Water sorption isotherms of neat CAU-10-H and CAU-10-H-GO_2, 5, 8, 15 wt% composites (at 293 K). Adsorption is depicted with filled, desorption with empty symbols. (a) Full region from p•p_0^{-1} = 0–1, (b) expanded adsorption region from p•p_0^{-1} = 0.25–0.5 (for clarity, only the adsorption isotherms are shown).

the idea together. **Marco Bengsch:** carried out preliminary experiments. **Alex Spieß:** collected the SEM images. **Carsten Schlüsener:** collected the SEM images. **Sandra Nießing:** collected the SEM images. **Christoph Janiak:** outlined the idea together.

Declaration of competing interest

The authors declare that they have no known competing financial interests or personal relationships that could have appeared to influence the work reported in this paper.

Acknowledgement

The authors gratefully acknowledge the financial support of the Federal German Ministry of Education and Research (BMBF) in the project Optimat under grant no. 03SF0492C.

Appendix A. Supplementary data

Supplementary data to this article can be found online at https://doi.org/10.1016/j.micromeso.2021.111352.

References

[1] S.R. Batten, N.R. Champness, X.-M. Chen, J. Garcia-Martinez, S. Kitagawa, L. Öhrström, M. O'Keeffe, M.P. Suh, J. Reedijk, Pure Appl. Chem. 85 (2013) 1715–1724.
[2] C. Janiak, J.K. Vieth, New J. Chem. 34 (2010) 2366–2388.
[3] C. Janiak, Dalton Trans. (2003) 2781–2804.
[4] H. Furukawa, N. Ko, Y.B. Go, N. Aratani, S.B. Choi, E. Choi, A.Ö. Yazaydin, R. Q. Snurr, M. O'Keeffe, J. Kim, O.M. Yaghi, Science 329 (2010) 424–428.
[5] O.K. Farha, A.Ö. Yazaydin, I. Eryazici, C.D. Malliakas, B.G. Hauser, M. G. Kanatzidis, S.T. Nguyen, R.Q. Snurr, J.T. Hupp, Nat. Chem. 2 (2010) 944–948.
[6] A.U. Czaja, N. Trukhan, U. Müller, Chem. Soc. Rev. 38 (2009) 1284–1293.
[7] J. Dechnik, J. Gascon, C.J. Doonan, C. Janiak, C.J. Sumby, Angew. Chem. Int. Ed. 56 (2017) 9292–9310.
[8] B. Li, H.-M. Wen, W. Zhou, B. Chen, J. Phys. Chem. Lett. 5 (2014) 3468–3479.
[9] J.Y. Lee, O.K. Farha, J. Roberts, K.A. Scheidt, S.T. Nguyen, J.T. Hupp, Chem. Soc. Rev. 38 (2009) 1450–1459.
[10] Y.-B. Huang, J. Liang, X.-S. Wang, R. Cao, Chem. Soc. Rev. 46 (2017) 126–157.
[11] A. Herbst, C. Janiak, CrystEngComm 19 (2017) 4092–4117.
[12] F. Jeremias, D. Fröhlich, C. Janiak, S.K. Henninger, New J. Chem. 38 (2014) 1846–1852.
[13] X. Liu, X. Wang, F. Kapteijn, Chem. Rev. 120 (2020) 8303–8377.
[14] C. Janiak, S.K. Henninger, Chimia 67 (2013) 419–424.
[15] S.K. Henninger, F.P. Schmidt, H.-M. Henning, Appl. Therm. Eng. 30 (2010) 1692–1702.
[16] D.M. Steinert, S.-J. Ernst, S.K. Henninger, C. Janiak, Eur. J. Inorg. Chem. (2020) 4502–4515.
[17] L.D. O'Neill, H. Zhang, D. Bradshaw, J. Mater. Chem. 20 (2010) 5720–5726.
[18] M.D. Rowe, D.H. Thamm, S.L. Kraft, S.G. Boyes, Biomacromolecules 10 (2009) 983–993.
[19] M. Arnold, P. Kortunov, D.J. Jones, Y. Nedellec, J. Kärger, J. Caro, Eur. J. Inorg. Chem. (2007) 60–64.
[20] J. Gascon, S. Aguado, F. Kapteijn, Microporous Mesoporous Mater. 113 (2008) 132–138.
[21] Y. Liu, Z. Ng, E.A. Khan, H.-K. Jeong, C.-B. Ching, Z. Lai, Microporous Mesoporous Mater. 118 (2009) 296–301.
[22] Y. Yoo, H.-K. Jeong, Chem. Commun. (2008) 2441–2443.
[23] S. Hermes, D. Zacher, A. Baunemann, C. Wöll, R.A. Fischer, Chem. Mater. 19 (2007) 2168–2173.
[24] S.J. Yang, J.Y. Choi, H.K. Chae, J.H. Cho, K.S. Nahm, C.R. Park, Chem. Mater. 21 (2009) 1893–1897.
[25] M. Jahan, Q. Bao, J.-X. Yang, K.P. Loh, J. Am. Chem. Soc. 132 (2010) 14487–14495.
[26] C. Petit, B. Mendoza, T.J. Bandosz, ChemPhysChem 11 (2010) 3678–3684.
[27] C. Petit, T.J. Bandosz, Adv. Funct. Mater. 21 (2011) 2108–2117.
[28] C. Petit, T.J. Bandosz, Dalton Trans. 41 (2012) 4027–4035.
[29] D. Bradshaw, A. Garai, J. Huo, Chem. Soc. Rev. 41 (2012) 2344–2381.
[30] I. Ahmed, S.H. Jhung, Mater. Today 17 (2014) 136–146.
[31] J. Yan, Y. Yu, C. Ma, J. Xiao, Q. Xia, Y. Li, Z. Li, Appl. Therm. Eng. 84 (2015) 118–125.
[32] W.S. Hummers, R.E. Offeman, J. Am. Chem. Soc. 80 (1958) 1339.
[33] X. Liu, H. Zhou, Y. Zhang, Y. Liu, A. Yuan, Chin. J. Chem. 30 (2012) 2563–2566.
[34] O.C. Compton, S.T. Nguyen, Small 6 (2010) 711–723.
[35] S. Park, J. An, I. Jung, R.D. Piner, S.J. An, X. Li, A. Velamakanni, R.S. Ruoff, Nano Lett. 9 (2009) 1593–1597.
[36] Y. Zhao, H. Ding, Q. Zhong, Appl. Surf. Sci. 284 (2013) 138–144.
[37] C. Petit, T.J. Bandosz, Adv. Funct. Mater. 20 (2010) 111–118.
[38] E. Elsayed, H. Wang, P.A. Anderson, R. Al-Dadah, S. Mahmoud, H. Navarro, Y. Ding, J. Bowen, Microporous Mesoporous Mater. 244 (2017) 180–191.
[39] I. Ahmed, N.A. Khan, S.H. Jhung, Inorg. Chem. 52 (2013) 14155–14161.
[40] C. Petit, T.L. Huang, J. Jagiello, J. Kenvin, K.E. Gubbins, T.J. Bandosz, Langmuir 27 (2011) 13043–13051.
[41] Y. Li, J. Miao, X. Sun, J. Xiao, Y. Li, H. Wang, Q. Xia, Z. Li, Chem. Eng. J. 298 (2016) 191–197.
[42] Y. Chen, D. Lv, J. Wu, J. Xiao, H. Xi, Q. Xia, Z. Li, Chem. Eng. J. 308 (2017) 1065–1072.
[43] S.-C. Wu, L.-L. Yu, F.-F. Xiao, X. You, C. Yang, J.-H. Cheng, J. Alloys Compd. 724 (2017) 625–632.
[44] Y. Zheng, S. Zheng, H. Xue, H. Pang, Adv. Funct. Mater. 28 (2018) 1804950.
[45] C. Petit, T.J. Bandosz, Adv. Mater. 21 (2009) 4753–4757.
[46] M.F. de Lange, K.J.F.M. Verouden, T.J.H. Vlugt, J. Gascon, F. Kapteijn, Chem. Rev. 115 (2015) 12205–12250.
[47] E. Hastürk, S.-J. Ernst, C. Janiak, Curr. Opinion Chem. Eng. 24 (2019) 26–36.
[48] S. Gökpinar, S.-J. Ernst, E. Hastürk, M. Möllers, I. El Aita, R. Wiedey, N. Tannert, S. Nießing, S. Abdpour, A. Schmitz, J. Quodbach, G. Füldner, S.K. Henninger, C. Janiak, Ind. Eng. Chem. Res. 58 (2019) 21493–21503.
[49] Y.I. Aristov, Appl. Therm. Eng. 50 (2013) 1610–1618.
[50] F. Jeremias, A. Khutia, S.K. Henninger, C. Janiak, J. Mater. Chem. 22 (2012) 10148–10151.
[51] C. Schlüsener, M. Xhinovci, S.-J. Ernst, A. Schmitz, N. Tannert, C. Janiak, Chem. Mater. 31 (2019) 4051–4062.
[52] N. Tannert, C. Jansen, S. Nießing, C. Janiak, Dalton Trans. 48 (2019) 2967–2976.
[53] C. Schlüsener, D.N. Jordan, M. Xhinovci, T.J. Matemb Ma Ntep, A. Schmitz, B. Giesen, C. Janiak, Dalton Trans. 49 (2020) 7373–7383.
[54] A. Khutia, H.U. Rammelberg, T. Schmidt, S.K. Henninger, C. Janiak, Chem. Mater. 25 (2013) 790–798.
[55] M. Thommes, K. Kaneko, A.V. Neimark, J.P. Olivier, F. Rodriguez-Reinoso, J. Rouquerol, K.S. Sing, Pure Appl. Chem. 87 (2015) 1051–1069.
[56] A. Vishnyakov, P. Ravikovitch, A.V. Neimark, Langmuir 16 (2000) 2311–2320.
[57] L.D. Gelb, K.E. Gubbins, R. Radhakrsihan, M. Sliwinska-Bartowiak, Rep. Prog. Phys. 62 (1999) 1573–1659.
[58] N.A. Sedron, J.P.R.B. Walton, N. Quirke, Carbon 27 (1989) 853–861.
[59] M. Qiu, Q. Guan, W. Li, Cryst. Growth Des. 16 (2016) 3639–3646.
[60] H. Reinsch, M.A. van der Veen, B. Gil, B. Marszalek, T. Verbiest, D. de Vos, N. Stock, Chem. Mater. 25 (2013) 17–26.
[61] F. Barroso-Bujans, S. Cerveny, A. Alegría, J. Colmenero, Carbon 48 (2010) 3277–3286.
[62] A. Buchsteiner, A. Lerf, J. Pieper, J. Phys. Chem. B 110 (2006) 22328–22338.
[63] B. Kartick, S.K. Srivastava, J. Nanosci. Nanotechnol. 11 (2011) 8586–8592.
[64] E. Tegou, G. Pseiropoulos, M.K. Filippidou, S. Chatzandroulis, Microelectron. Eng. 159 (2016) 146–150.
[65] D.R. Dreyer, S. Park, C.W. Bielawski, R.S. Ruoff, Chem. Soc. Rev. 39 (2010) 228–240.
[66] C. Volkringer, D. Popov, T. Loiseau, G. Férey, M. Burghammer, C. Riekel, M. Haouas, F. Taulelle, Chem. Mater. 21 (2009) 5695–5697.
[67] D. Fröhlich, E. Pantatosaki, P.D. Kolokathis, K. Markey, H. Reinsch, M. Baumgartner, M.A. van der Veen, D.E. De Vos, N. Stock, G.K. Papadopoulos, J. Mater. Chem. A 4 (2016) 11859–11869.
[68] D. Fröhlich, S.K. Henninger, C. Janiak, Dalton Trans. 43 (2014) 15300–15304.
[69] X. Zhou, W. Huang, J. Miao, Q. Xia, Z. Zhang, H. Wang, Z. Li, Chem. Eng. J. 266 (2015) 339–344.